Comparative Evaluation of Serotonin Transporter Radioligands ^{11}C-DASB and ^{11}C-McN 5652 in Healthy Humans

W. Gordon Frankle, MD[1]; Yiyun Huang, PhD[1,2]; Dah-Ren Hwang, PhD[1,2]; Peter S. Talbot, MD[1]; Mark Slifstein, PhD[1]; Ronald Van Heertum, MD[2]; Anissa Abi-Dargham, MD[1,2]; and Marc Laruelle, MD[1,2]

[1]Department of Psychiatry, Columbia University College of Physicians and Surgeons, and the New York State Psychiatric Institute, New York, New York; and [2]Department of Radiology, Columbia University College of Physicians and Surgeons, and the New York State Psychiatric Institute, New York, New York

Alterations of serotonin transporters (SERT) are implicated in a large number of psychiatric conditions. ^{11}C-(+)-6β-(4-Methylthiophenyl)-1,2,3,5,6α,10β-hexahydropyrrolo[2,1-a]isoquinoline (^{11}C-McN 5652) was the first PET radiotracer successfully developed as a SERT imaging agent. Recently, ^{11}C-3-amino-4-(2-dimethylaminomethylphenylthio)benzonitrile (^{11}C-DASB) was introduced as an alternative to ^{11}C-McN 5652. Comparative evaluation of ^{11}C-DASB and ^{11}C-McN 5652 in baboons indicates that ^{11}C-DASB is associated with (a) lower nonspecific binding in the brain, (b) higher plasma free fraction, and (c) faster plasma clearance and brain uptake kinetics, enabling measurement of SERT parameters in a shorter scanning time. The purpose of this study was to compare these 2 agents in healthy humans. **Methods:** Six healthy volunteers underwent 2 PET scans on the same day, one with ^{11}C-DASB and one with ^{11}C-McN 5652, in counterbalanced order. Regional distribution volumes (V_T) were derived for 16 brain regions by kinetic analysis using the arterial input function. **Results:** Both ^{11}C-DASB and ^{11}C-McN 5652 displayed similar patterns of accumulation: highest levels in the midbrain, thalamus and striatum; intermediate in the limbic regions; low in the neocortex; and lowest in the cerebellum. ^{11}C-DASB cerebellar V_T (10.1 ± 2.0 mL g^{-1}) was lower than that of ^{11}C-McN 5652 (20.8 ± 3.6 mL g^{-1}), indicating lower nonspecific binding. As a result, regional specific-to-nonspecific equilibrium partition coefficients (V_3'') of ^{11}C-DASB were higher compared with those of ^{11}C-McN 5652 (for example, midbrain V_3'' of ^{11}C-DASB and ^{11}C-McN 5652 were 2.04 ± 0.44 and 1.20 ± 0.34, respectively). The plasma free fraction was 8.9% ± 1.6% for ^{11}C-DASB and was not measurable for ^{11}C-McN 5652. In contrast to the situation observed in baboons, plasma clearances of both compounds were similar in humans, and the minimal scanning times required to derive time-invariant distribution volumes in all regions were comparable for both tracers (95 min). **Conclusion:** With the exception of the scanning time, predictions from baboon studies were confirmed in humans. The higher specific-to-nonspecific ratios of ^{11}C-DASB are a critical advantage. This property will be especially important for the measurement of SERT in regions with moderate density, such as the limbic regions, where alterations of serotonin transmission might be associated with anxiety and depression.

Key Words: serotonin transporter; ^{11}C-3-amino-4-(2-dimethylaminomethylphenylthio)benzonitrile; ^{11}C-(+)-6β-(4-methylthiophenyl)-1,2,3,5,6α,10β-hexahydropyrrolo[2,1-a]isoquinoline; PET

J Nucl Med 2004; 45:682–694

Alterations of serotonin (5-HT) transmission play a role in a variety of psychiatric conditions including major depression, obsessive compulsive, and other anxiety disorders as well as schizophrenia. The importance of the 5-HT transporter (SERT) in regulating 5-HT function, along with the fact that this receptor is the site of action of most antidepressant medications, has led to significant interest in developing PET radiotracers for this target. In the human brain, SERT is present in high density in the midbrain area, the thalamus, and the striatum; moderate density in the limbic regions such as amygdala, hippocampus, and cingulate cortex; and low density in the neocortical regions (*1–3*).

^{11}C-(+)-6β-(4-Methylthiophenyl)-1,2,3,5,6α,10β-hexahydropyrrolo[2,1-a]isoquinoline (^{11}C-McN 5652) was the first PET radiotracer successfully developed to image SERT density in humans (*4–8*). This radiotracer has been used in several clinical studies, including studies of patients with mood disorders (*9*), obsessive compulsive disorder (*10*), and ecstasy abuse (*11,12*). However, ^{11}C-McN 5652 is not without some limitations (*7*). First, its nonspecific binding is relatively high, thus precluding the reliable quantification of SERT in regions of moderate-to-low SERT density. Second, the plasma free fraction is too low to be measured with accuracy using traditional ultracentrifugation methods, making it difficult to control for this variable in clinical studies. Finally, the brain uptake of this radiotracer is protracted, so that long imaging sessions are required to derive accurate SERT binding parameters.

More recently, Wilson and coworkers introduced ^{11}C-3-amino-4-(2-dimethylaminomethylphenylthio)benzonitrile

Received Jul. 23, 2003; revision accepted Nov. 17, 2003.
For correspondence or reprints contact: W. Gordon Frankle, MD, New York State Psychiatric Institute, 1051 Riverside Dr., Box 31, New York, NY 10032.
E-mail: wf2004@columbia.edu

(^{11}C-DASB) as a new PET radiotracer suitable to image SERT (*13–17*). Two studies compared the imaging qualities of ^{11}C-McN 5652 and ^{11}C-DASB in baboons and concluded that ^{11}C-DASB provided significant improvement over ^{11}C-McN 5652, for it has higher specific-to-nonspecific binding ratios, higher plasma free fraction, and faster uptake kinetics (*18*,*19*).

The aim of this study was to compare ^{11}C-DASB and ^{11}C-McN 5652 as imaging agents for the SERT in healthy humans. This characterization was performed in the same subjects, under standardized conditions, to facilitate an unbiased comparison. Six individuals were studied twice on the same day, once with each radiotracer, administered in a counterbalanced order. The main purpose of this study was to evaluate if the improved properties of ^{11}C-DASB relative to ^{11}C-McN 5652 observed in baboons were confirmed in healthy human subjects.

MATERIALS AND METHODS

Human Subjects

The study was approved by the Institutional Review Boards of the New York State Psychiatric Institute and Columbia Presbyterian Medical Center. Six healthy volunteers participated in this study (4 males, 2 females; age, 27 ± 6 y; range, 18–34 y; these and subsequent values are given as mean ± SD). The absence of pregnancy, medical, neurologic, and psychiatric history (including alcohol and drug abuse) was assessed by history, review of systems, physical examination, and routine blood tests, including pregnancy test, urine toxicology, and electrocardiogram. Subjects provided written informed consent after receiving an explanation of the study.

Radiochemistry

^{11}C-DASB. The standard DASB and precursor desmethyl DASB were a gift from the University of Toronto. Preparation of ^{11}C-DASB followed the literature procedure, with some modifications (*13*).

Desmethyl DASB was dissolved in 0.3 mL of *N*,*N*-dimethylformamide (DMF) and the solution was cooled to −20°C to −10°C. ^{11}C-Methyl iodide, produced according to the literature procedure (*20*), was bubbled into the cooled precursor solution. When maximum radioactivity was collected in the reaction vial, the bubbling line was removed from the vial. The reaction mixture was then heated at 80°C for 5 min, mixed with 0.4 mL of H_2O, and injected onto a semipreparative high-pressure liquid chromatography (HPLC) column (Prodigy ODS-prep, 10 μm, 250 × 10 mm; Phenomenex; mobile phase, 40% MeCN/60% 0.1 mol/L $NH_4CH_3CO_2$; flow rate, 10 mL/min; retention time for ^{11}C-DASB, 12 min).

The HPLC fraction containing ^{11}C-DASB was diluted with 100 mL of H_2O and passed through a C_{18} SepPak column (Waters Corp.), preconditioned by washing with 5 mL of EtOH followed by 5 mL of H_2O. The SepPak column was rinsed with 10 mL of H_2O and the product was eluted off with 1 mL of EtOH. A small sample of the EtOH solution (10–30 mL) was injected onto an analytic HPLC column (Prodigy ODS-3, 5 μm, 250 × 4.6 mm; Phenomenex; mobile phase, 35% MeCN/65% 0.1 mol/L NH_4HCO_2 solution; flow rate, 2 mL/min; retention time for ^{11}C-DASB, 7.8 min) to determine the radiochemical purity, chemical purity, and specific activity of the product. The remaining EtOH solution was then diluted with 9 mL of saline, filtered through a membrane filter (Millex GV, 0.22 μm, 25 mm; Millipore Corp.), and collected in a sterile vial.

The chemical purity of ^{11}C-DASB was >99%. The radiochemical purity was >90%.

^{11}C-MCN 5652. The standard (+)-McN 5652 was a gift from R.W. Johnson Pharmaceutical Research Institute. The precursor for the production of ^{11}C- (+)-McN 5652, (+)-McN butyryl thioester tartrate, was prepared from (+)-McN 5652 by a modified literature procedure (*21*).

Briefly, (+)-McN 5652 in anhydrous tetrahydrofuran was reacted with sodium and liquid ammonia at −78°C for 20 min to provide the thiophenol, which was converted to the butyryl thioester by reaction with butyryl chloride at room temperature for 5 min. The crude reaction product was purified by column chromatography on silica gel. The resulting thioester was stabilized and further purified by treatment with tartaric acid to provide the stable (+)-McN butyryl thioester tartrate, which was >96% chemically and >98% optically pure, as indicated by reverse-phase and chiral HPLC analyses using the published analytic procedures (*22*).

To a reaction vial containing 0.5 mg of the precursor (+)-McN butyryl thioester tartrate was added 0.3 mL of DMF and 10 μL of tetrabutylammonium hydroxide (1.0 mol/L solution in MeOH). ^{11}C-Methyl iodide was bubbled into the precursor solution at room temperature. When maximum radioactivity was collected in the reaction vial, the reaction mixture was heated at 60°C for 2 min. Purification and processing procedures of ^{11}C-(+)-McN 5652 were the same as those for ^{11}C-DASB (Semipreparative HPLC column: Prodigy C_{18} ODS-prep, 10 μm, 250 × 10 mm; mobile phase, 30% MeCN/70% 0.1 mol/L NH_4HCO_2 solution; flow rate, 15 mL/min; retention time of ^{11}C-(+)-McN 5652, 16 min. Analytic HPLC column: Prodigy C_{18} ODS-3, 5 μm, 250 × 4.6 mm; mobile phase, 40% MeCN/60% 0.1 mol/L NH_4HCO_2 solution; flow rate, 2 mL/min; retention time of ^{11}C-(+)-McN 5652, 8.5 min).

The radiochemical and chemical purity of ^{11}C-(+)-McN 5652 in saline was >95%.

PET Protocol

All subjects were studied with ^{11}C-DASB and ^{11}C-McN 5652 on the same day. The injection order was counterbalanced. Three subjects were scanned with ^{11}C-DASB first, and 3 subjects were scanned with ^{11}C-McN 5652 first. An arterial catheter was inserted in the radial artery after completion of the Allen test and infiltration of the skin with 1% lidocaine. A venous catheter was inserted in a forearm vein on the opposite side. Head movement minimization was achieved with a polyurethane head immobilization system (Soule Medical, FA) (*23*). PET imaging was performed with the ECAT EXACT HR+ (Siemens/CTI) (63 slices covering an axial field of view [FOV] of 15.5 cm, axial sampling of 3.46 mm, 3-dimensional [3D] mode in plane and axial resolution of 4.4 and 4.1 mm full width at half maximum at the center of the FOV, respectively). A 10-min transmission scan was obtained before radiotracer injection. Radiotracers were injected intravenously over 30 s. Emission data were collected in the 3D mode for 120 min as 21 successive frames of increasing duration (3 × 20 s, 3 × 1 min, 3 × 2 min, 2 × 5 min, 10 × 10 min). Subjects were allowed to rest outside of the camera for 30–45 min between the 2 injections.

Input Function Measurement

After radiotracer injection, arterial samples were collected every 10 s with an automated sampling system for the first 2 min and collected manually thereafter at longer intervals. A total of 32 samples were obtained per scan. After centrifugation (10 min at 1,800*g*), plasma was collected in 200-μL aliquots and activities were counted in a γ-counter (Wallac 1480 Wizard 3M Automatic γ-Counter).

Seven samples (collected at 2, 16, 30, 50, 70, 90, and 120 min) were further processed by HPLC to measure the fraction of plasma activity representing unmetabolized parent compound. For ^{11}C-DASB, plasma samples (0.5 mL) were added to 1.0 mL of MeOH in a centrifuge tube. After mixing, the samples were centrifuged at 15,000 rpm for 3.5 min. The liquid phase was separated from the precipitate. Activity in 0.1 mL of the liquid phase was counted and the remainder was injected onto the HPLC column. For ^{11}C-McN 5652, 1-mL aliquots of plasma were loaded onto a C_{18} SepPak column (Waters classic; Waters) preconditioned with 5 mL of MeOH and 10 mL of water. The SepPak was flushed with air, washed with 5 mL of water, and eluted with 1 mL of MeOH.

The HPLC system consisted of a Waters 510 isocratic pump, a Rheodyne injector with a 2-mL sample loop, a Phenomenex C_{18} ODS column (10-μm particle size, 250 × 4.6 mm), and a γ-detection system (Bioscan Flow Count Unit). The column was eluted with a solvent mixture of acetonitrile/0.1 mol/L aqueous ammonium formate (30:70) at a flow rate of 2.5 mL/min. The HPLC eluate was collected in either 5 (for ^{11}C-McN 5652) or 7 (for ^{11}C-DASB) counting tubes (4.0 mL each). A standard was processed with each sample to determine the retention time of the unmetabolized compound. For each sample, the unmetabolized fraction was estimated by the ratio of activity, decay corrected, in the parent peak to the total activity. A biexponential function was fitted to the 7 measured unmetabolized fractions that was then used to interpolate values between the measurements. The smallest exponential of the unmetabolized fraction curve, λ_{par}, was constrained to the difference between λ_{cer}, the terminal rate of washout of cerebellar activity, and λ_{tot}, the smallest elimination rate constant of the total plasma activity (*24*).

The input function was calculated as the product of total counts and interpolated unmetabolized fraction at each time point. The measured input function values ($C_a(t)$, MBq/mL) were fitted to a sum of 3 exponentials from the time of peak plasma activity, and the fitted values were used as the input to the kinetic analysis. The initial distribution volume (V_{bol}, L) was calculated as the ratio of injected dose to peak plasma parent concentration. The clearance of the parent compound (C_L, l/h) was calculated as the ratio of the injected dose to the area under the curve of the input function (*25*).

For the determination of the plasma free fraction (f_1), triplicate 200-μL aliquots of plasma collected before injection were mixed with the radiotracer, pipetted into ultrafiltration units (Amicon Centrifree; Millipore), and centrifuged at room temperature (20 min at 4,000 rpm). At end of centrifugation, the plasma and ultrafiltrate activities were counted, and f_1 was calculated as the ratio of activity in the ultrafiltrate to total activity (*26*). Triplicate aliquots of saline solution mixed with the radiotracer were also processed to determine the filter retention of the free tracer. Plasma f_1 was determined only for ^{11}C-DASB, as the high retention (>90%) of free ^{11}C-McN 5652 on the filter impairs the free fraction measurement of ^{11}C-McN 5652 with this method (*7*).

MRI Acquisition and Segmentation Procedures

MR images were acquired on a General Electric 1.5-T Signa Advantage system. After a sagittal scout (localizer) image, performed to identify the anterior commissure–posterior commissure (AC–PC) plane (1 min), a transaxial T1-weighted sequence with 1.5-mm slice thickness was acquired in a coronal plane orthogonal to the AC–PC plane over the whole brain with the following parameters: 3D spoiled gradient recalled acquisition in the steady state; repetition time, 34 ms; echo time, 5 ms; flip angle, 45°; slice thickness, 1.5 mm and zero gap; 124 slices; FOV, 22 × 16 cm; with 256 × 192 matrix, reformatted to 256 × 256, yielding a voxel size of 1.5 × 0.9 × 0.9 mm; and time of acquisition, 11 min.

MRI segmentation was performed within MEDx (Sensor Systems, Inc.), with original subroutines implemented in MATLAB (The Math Works, Inc.). Steps for MRI segmentation included correction for field inhomogeneities, fitting of the intensity distribution to a sum of 3 gaussian functions, voxel classification, and postfiltering (*27*).

Image Analysis

Images were reconstructed to a 128 × 128 matrix (pixel size of 2.5 × 2.5 mm^2). Reconstruction was performed with attenuation correction using the transmission data and a Shepp 0.5 filter (cutoff, 0.5 cycle per projection ray). Reconstructed image files were then processed with the image analysis software MEDx. If indicated by visual inspection, frames were realigned to a frame of reference, using a least-squares algorithm for within-modality coregistration (automated image registration [AIR]) (*28*). The results of the frame-to-frame realignment were checked again visually. After frame-to-frame registration, the 21 frames were summed to one dataset, which was coregistered to the MRI dataset using AIR (*28*). The spatial transformation derived from the summed PET registration procedure was then applied to each individual frame. Thus, each PET frame was resampled in the coronal plane to a voxel volume of 1.5 × 0.9 × 0.9 mm^3.

Regions of interest ([ROIs], n = 16) and region of reference (cerebellum) boundaries were drawn on the MR image according to criteria derived from brain atlases (*29*,*30*) and published reports (*31*–*34*). A segmentation-based method was used for the neocortical regions, and a direct identification method was used for the subcortical regions.

For the neocortical regions, large regions were first drawn to delineate the boundaries of the ROIs. Within these regions, only the voxels classified as gray matter were used to measure the activity distribution. Sampled volumes of the neocortical regions (n = 7) were as follows: dorsolateral prefrontal cortex (DLPFC, 26,027 ± 3,244 mL^3), medial prefrontal cortex (MPFC, 6,417 ± 1,206 mL^3), orbitofrontal cortex (OFC, 14,472 ± 2,341 mL^3), anterior cingulate cortex (ACC, 3,455 ± 1,160 mL^3), parietal cortex (PC, 56,728 ± 3,408 mL^3), temporal cortex (TC, 50,013 ± 3,785 mL^3), and occipital cortex (OC, 36,056 ± 6,386 mL^3).

Because of the mixture of gray and white matter in the central gray structures (especially in the thalamus), the segmentation-based approach was not used to define the subcortical ROIs, and the boundaries of these regions were identified by anatomic criteria. The subcortical regions (n = 10) included caudate (CAU, 7,412 ± 1,423 mL^3), putamen (PUT, 9,910 ± 1,858 mL^3), ventral striatum (VST, 2,653 ± 823 mL^3), thalamus (THA, 9,228 ± 1,896 mL^3), midbrain (MID, 7,513 ± 1,582 mL^3), amygdala (AMY, 4,936 ± 718 mL^3), entorhinal cortex (ENT, 2,421 ± 564 mL^3), parahippocampal gyrus (PAR, 8,660 ± 1,026 mL^3), hippocampus

(HIP, 8,514 ± 632 mL^3), and cerebellum (CER, 35,062 ± 12,450 mL^3).

For bilateral regions, right and left values were averaged. The contribution of plasma total activity to the regional activity was calculated assuming a 5% blood volume in the ROIs (*35*), and tissue activities were calculated as the total regional activities minus the plasma contribution.

Derivation of Distribution Volumes

Derivation of ^{11}C-DASB and ^{11}C-MCN 5652 regional tissue distribution volumes (V_T, mL g^{-1}) was performed with kinetic modeling using the arterial input function and a 2-compartment model (i.e., 1-tissue-compartment model [1TC model]). This model has been demonstrated to provide reliable estimates of V_T for both ^{11}C-DASB (*17*) and ^{11}C-MCN 5652 (*7*). V_T, which is equal to the ratio of tissue to plasma parent activity at equilibrium, was derived as the K_1/k_2 ratio, where K_1 (mL g^{-1} min^{-1}) and k_2 (min^{-1}) are the unidirectional fractional rate constants for the transfer of the tracer in and out of the brain, respectively (*36*,*37*). Kinetic parameters were derived by nonlinear regression using a Levenberg–Marquart least-squares minimization procedure (*38*) implemented in MATLAB (The Math Works, Inc.), as previously described (*36*). Given the unequal sampling over time (increasing frame acquisition time from the beginning to the end of the study), the least-squares minimization procedure was weighted by the frame acquisition time.

The minimal scanning time required to achieve time-independent derivation of regional V_T was evaluated by fitting the time–activity curves to shorter datasets, representing a total scanning time of 110, 100, 90, 80, 70, 60, 50, 40, and 30 min, respectively. The resulting estimates of V_T were normalized to the V_T derived with the 120-min dataset. The average and SD of the normalized V_T were calculated for each scan duration. Time independence was considered achieved at time t if, for the frame ending at time t and all subsequent frames, the following 2 criteria were fulfilled: (a) the average normalized V_T was between 95% and 105% of the reference V_T (small bias); and (b) the SD of the normalized V_T was <10% (small error). These criteria were similar to the ones previously used in baboons (*18*).

Derivation of SERT Parameters

Derivation of SERT parameters was based on the following assumptions: (a) because of the negligible density of SERT in the cerebellum (*1*–*3*), cerebellum V_T was assumed to be representative of equilibrium nonspecific binding; and (b) the nonspecific binding did not vary significantly between regions.

The binding potential ([BP], mL g^{-1}) was derived as the difference between V_T in the ROI ($V_{T\ ROI}$) and V_T in the cerebellum ($V_{T\ CER}$), the reference region. The relationship between BP and SERT receptor parameters was given by (*39*):

$$BP = \frac{f_1 B_{max}}{K_d},$$

where B_{max} is the regional concentration of SERT (nmol/L), and K_d is the in vivo affinity of the tracer for SERT (nmol/L).

The specific-to-nonspecific equilibrium partition coefficient (V_3'') was derived as the ratio of BP to $V_{T\ CER}$. The relationship between V_3'' and SERT receptor parameters is given by (*39*):

$$V_3'' = \frac{f_2 B_{max}}{K_d},$$

where f_2 is the free fraction of the nonspecific distribution volume in the brain ($f_2 = f_1/V_{T\ CER}$). V_3'' provides a measure of the signal-to-noise contrast associated with the detection of specific binding. In contrast to simple tissue activity ratios, V_3'' is independent of the time of measurement.

Statistical Analysis

Dependent variables were analyzed using repeated-measures ANOVA (RM ANOVA), with tracer as repeated condition and, when appropriate, regions as cofactors. A 2-tailed probability value of 0.05 was selected as the significance level. This design gives differences due to the radiotracer, after taking into account individual differences. Thus, using this analysis, we determined the significance level of between-tracer differences.

RESULTS

Injected Dose

The injected dose did not differ between ^{11}C-DASB and ^{11}C-MCN 5652 (547.6 ± 122.1 MBq vs. 410.7 ± 140.6 MBq, respectively; RM ANOVA, $P = 0.09$). The injected mass also did not differ between ^{11}C-DASB and ^{11}C-MCN 5652 (4.5 ± 1.3 μg vs. 5.2 ± 0.3 μg, respectively; RM ANOVA, $P = 0.25$). The specific activity of ^{11}C-DASB (3,544 ± 873 GBq/mmol) was significantly higher than that of ^{11}C-MCN 5652 (2,298 ± 696 GBq/mmol; RM ANOVA, $P = 0.02$).

Plasma Analysis

After an initial, rapid distribution phase, plasma activity stabilized at relatively constant levels for both tracers. During this plateau phase, total plasma activity was higher after ^{11}C-DASB injection (Fig. 1). Both radiotracers underwent significant metabolism over the duration of the study (Fig. 2). A significant difference in the rate of metabolism was seen between tracers, with ^{11}C-DASB showing faster metabolism than ^{11}C-MCN 5652 (RM ANOVA, $P = 0.0008$). The initial peak of parent compound was higher for ^{11}C-MCN 5652 than for ^{11}C-DASB (Fig. 3, inset). Thus, the initial distribution volume (V_{bol}) of ^{11}C-DASB (46 ± 9 L) was significantly higher than that of ^{11}C-MCN 5652 (16 ± 4 L; RM ANOVA, $P = 0.008$). After the initial distribution phase, ^{11}C-MCN 5652 parent concentration became lower than that of ^{11}C-DASB parent concentration. No significant difference in the parent plasma clearance rate was observed between ^{11}C-DASB (159 ± 34 L h^{-1}) and ^{11}C-MCN 5652 (170 ± 53 L h^{-1}; RM ANOVA, $P = 0.64$) nor was a significant difference observed in the terminal half-life (^{11}C-DASB, 69 ± 42 min; ^{11}C-MCN 5652, 88 ± 55 min; RM ANOVA, $P = 0.49$). The free fraction of ^{11}C-DASB dissolved in saline was 95% ± 4%, indicating negligible retention on the ultracentrifugation filter. The free fraction of ^{11}C-DASB in the plasma was 8.9% ± 1.6%.

Brain Analysis

Regional Uptake. The activity of both tracers displayed similar patterns of accumulation (Fig. 4). Activity concentrated in regions with high SERT densities (midbrain, thalamus, and striatum). Intermediate levels of activity were

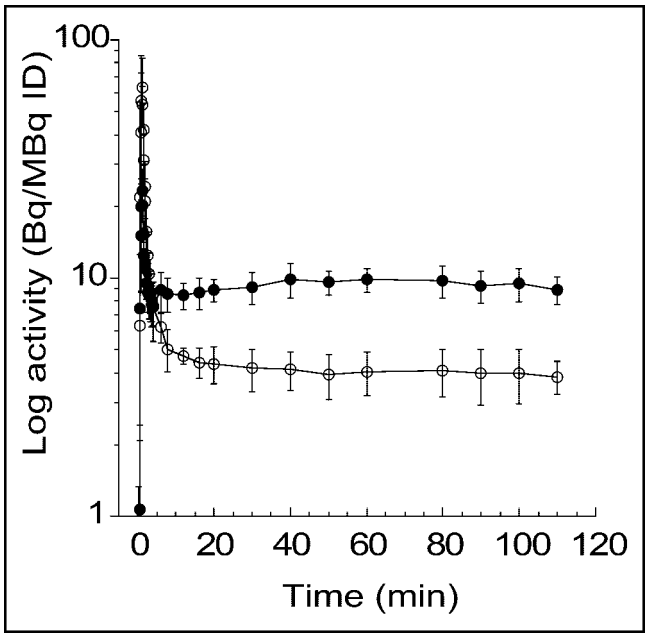

FIGURE 1. Mean ± SD of total plasma activity normalized to injected dose (ID) after injection of ^{11}C-DASB (●) and ^{11}C-McN 5652 (○). Each point is mean of 6 experiments. After rapid distribution, plasma activity stabilized to relatively constant level for both tracers. During plateau phase, higher activity was observed for ^{11}C-DASB than for ^{11}C-McN 5652.

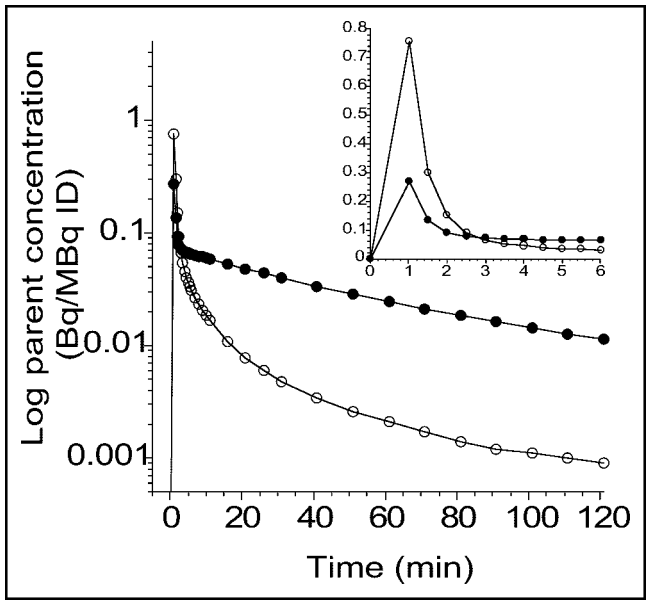

FIGURE 3. Mean plasma activity corresponding to parent compound after injection of ^{11}C-DASB (●) and ^{11}C-McN 5652 (○). Each point is mean of 6 experiments. Initial peak concentration of ^{11}C-McN 5652 was higher than that of ^{11}C-DASB (inset), which may represent greater binding to peripheral receptors for ^{11}C-DASB. After 3 min, concentration of ^{11}C-McN 5652 became lower than that of ^{11}C-DASB. ID = injected dose.

seen in the amygdala, hippocampus, cingulate, and parahippocampal gyrus. Lower levels were observed in the neocortex and cerebellum. Radiotracer accumulation in the central SERT- rich regions was readily noticeable with both tracers.

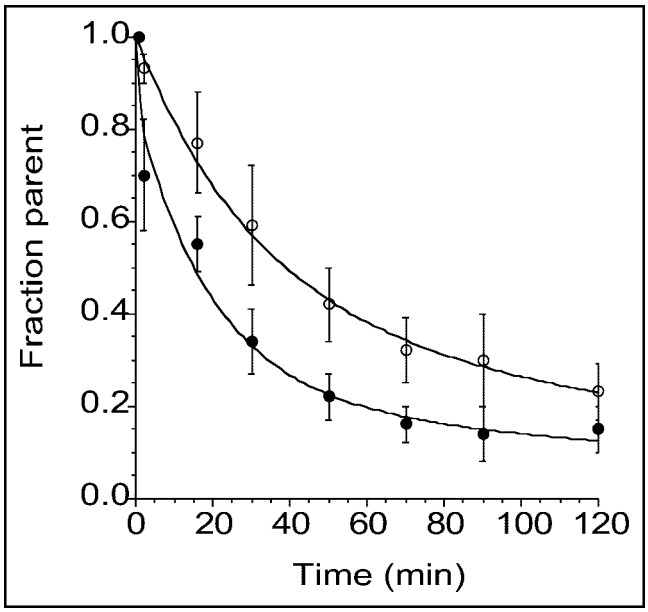

FIGURE 2. Mean ± SD of fraction of plasma activity corresponding to parent compound after injection of ^{11}C-DASB (●) and ^{11}C-McN 5652 (○). Values are mean of 6 experiments. Fraction parent of ^{11}C-DASB exhibited significantly faster reduction than that of ^{11}C-McN 5652 (P = 0.001).

The ^{11}C-DASB image provided improved contrast and finer details. For example, the higher accumulation in the dorsal raphe compared with the other regions of the midbrain is visually appreciable on the ^{11}C-DASB scan but not on the ^{11}C-McN 5652 scan (Fig. 4, bottom row). The amygdalae are also visible on the ^{11}C-DASB image but not on the ^{11}C-McN 5652 image.

Differences in brain uptake of ^{11}C-DASB and ^{11}C-McN 5652 are illustrated in Figure 5, which presents the time–activity curves for ^{11}C-DASB and ^{11}C-McN 5652 in representative brain regions recorded in the same subject on the same day for 120 min. The ^{11}C-DASB uptake displayed a well-defined peak, followed by rapid washout in all regions, whereas the ^{11}C-McN 5652 uptake was more protracted. Corresponding specific-to-nonspecific ratios are shown in Figure 6 and are notably higher for ^{11}C-DASB than for ^{11}C-McN 5652. Visual inspection of Figure 5 reveals that the fit is not perfect for either ^{11}C-DASB or ^{11}C-McN 5652, with nonrandom distribution of the residuals. For ^{11}C-DASB, the 1TC model-fitted curve tends to fall below the early data points, above the intermediate time points, and below the late time points. A similar pattern is seen with ^{11}C-McN 5652. However, using a higher-order model (e.g., a 2-tissue-compartment model [2TC model]) does not offer significant improvement in the fit over the 1TC for either ^{11}C-DASB (data not shown (*17*)) or for ^{11}C-McN 5652 (*7*).

Table 1 lists the regional peak uptake times, the rate of tracer washout, and the time of peak specific binding for the different regions. Peak uptake time was calculated as the

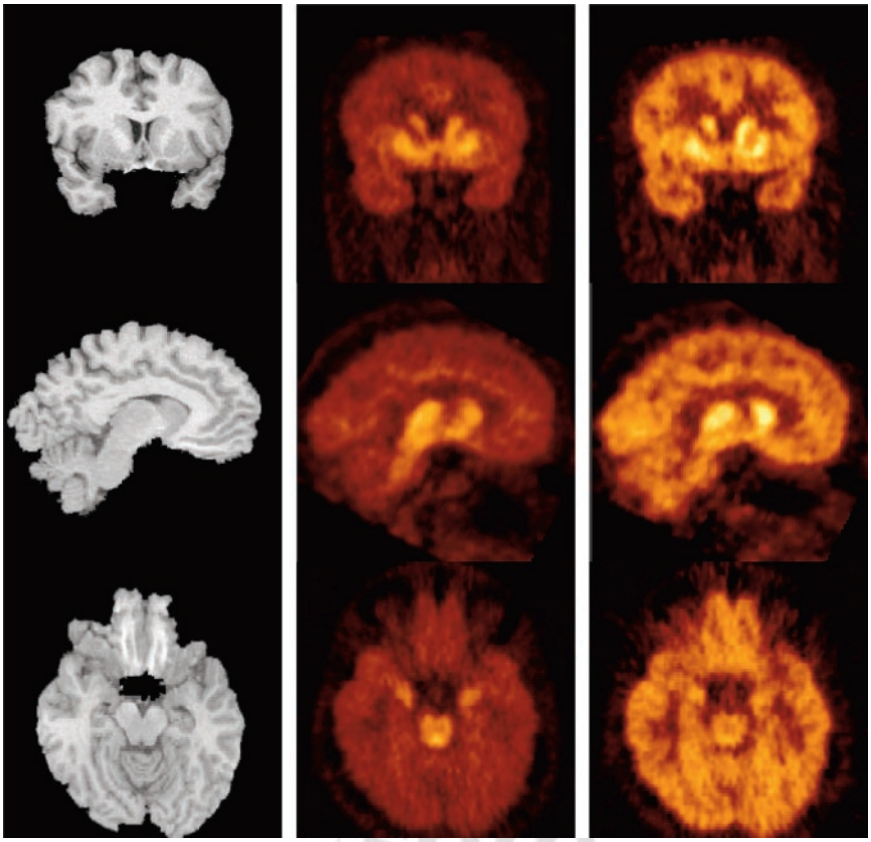

FIGURE 4. MR images (left) and coregistered PET images acquired from 40 to 90 min after injection of 659 MBq ^{11}C-DASB (center) and 599 MBq ^{11}C-McN 5652 (right) in 33-y-old healthy male volunteer. Activity was normalized to injected dose and color coded using identical scale. (Top row) Coronal plane illustrates ventrodorsal gradient of SERT in striatum. (Middle row) Sagittal plane close to midline shows accumulation of activity in thalamus and caudate. Image also illustrates low level of activity in cerebellum and small difference in uptake between cerebellum and neocortical regions. (Bottom row) Transaxial plane at level of midbrain. Note very high activity concentration in dorsal raphe on ^{11}C-DASB scan, just ventral to fourth ventricle. Concentration of activity in amygdala is also noticeable on ^{11}C-DASB image.

maximum value of the curve fit to the time–activity data for each region using a 1TC kinetic model. The mean regional peak uptake times for ^{11}C-DASB and ^{11}C-McN 5652 were 42 ± 15 and 61 ± 23 min, respectively. RM ANOVA revealed significant differences in peak uptake between tracers ($P < 0.0001$) and between regions ($P < 0.0001$) with no significant tracer-by-region interaction ($P = 0.48$).

The fraction of tracer washout during the scan was estimated by calculating the relative decrease in regional activity over the time course of the scan relative to peak uptake (percentage decrease from peak to end of scan). The mean fractional regional washout rates for ^{11}C-DASB and ^{11}C-McN 5652 were 46% ± 21% and 16% ± 14%, respectively. RM ANOVA revealed significant differences in fractional activity washout between tracers ($P < 0.0001$) and between regions ($P < 0.0001$) with no significant tracer-by-region interaction ($P = 0.87$).

The time of peak specific binding was determined using a 2TC model to derive the component of specific binding for each region in the dataset. In this model, the nonspecific distribution volume was fixed to the value of cerebellum V_T, by constraining the K_1/k_2 ratio. The mean times of peak

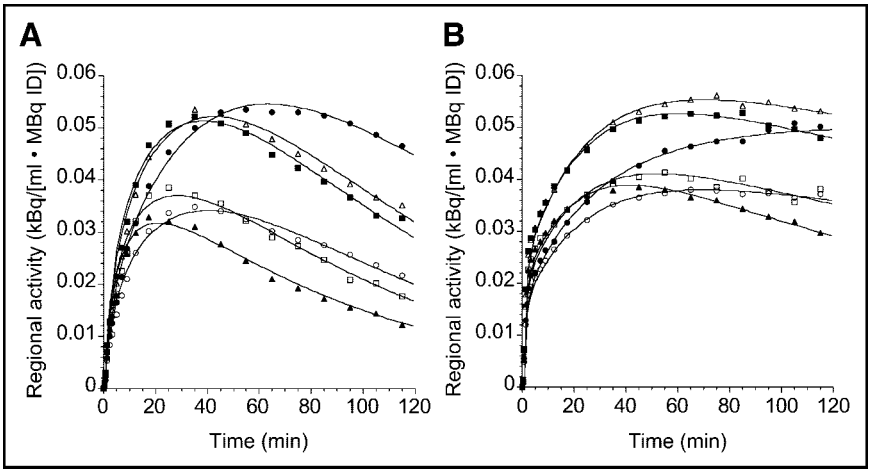

FIGURE 5. Time–activity curves of ^{11}C-DASB (A) and ^{11}C-McN 5652 (B) measured on same day in same human subject. Regions displayed include midbrain (●), thalamus (■), striatum (△), medial temporal lobe (○), anterior cingulate cortex (□), and cerebellum (▲). Points are measured activities in ROIs; lines are fitted values to 1TC model. *y*-Axis scale has been kept constant. Compared with ^{11}C-McN 5652, ^{11}C-DASB displays faster kinetics of uptake, with better-defined peak uptake and rapid washout. ID = injected dose.

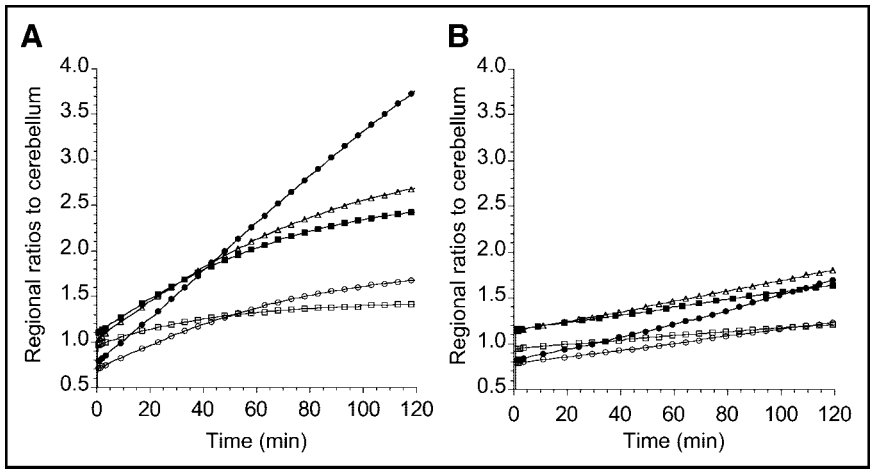

FIGURE 6. Ratios of ROIs to cerebellum of ^{11}C-DASB (A) and ^{11}C-McN 5652 (B) measured on same day in same human subject (same experiment as presented in Fig. 5). Regions displayed include midbrain (●), thalamus (■), striatum (△), medial temporal lobe (○), and anterior cingulate cortex (□). *y*-Axis scale has been kept constant. ^{11}C-DASB displays enhanced tissue-to-cerebellum ratios compared with ^{11}C-McN 5652.

specific binding for ^{11}C-DASB and ^{11}C-McN 5652 were 40 ± 15 and 56 ± 24 min, respectively. RM ANOVA revealed significant differences in peak uptake between tracers ($P < 0.0001$), a significant difference between regions ($P < 0.0001$), and no tracer-by-region interaction ($P = 0.86$).

Kinetic Rate Constants. Overall, ^{11}C-DASB had a higher K_1 and k_2 (0.391 ± 0.06 mL g^{-1} min^{-1} and 0.028 ± 0.010 min^{-1}, respectively, average of all regions and all subjects) than ^{11}C-McN 5652 (0.304 ± 0.05 mL g^{-1} min^{-1} and 0.011 ± 0.004 min^{-1}, respectively, average of all regions and all subjects). Regional values of K_1 and k_2 are presented in Table 2. For K_1, RM ANOVA revealed significant between-tracer ($P < 0.0001$) and between-region ($P < 0.003$) differences, with no tracer-by-region interaction ($P = 0.99$). A significant tracer-by-subject interaction was also noted ($P < 0.0001$). A significant between-tracer and between-region difference was observed in the regional values of k_2 ($P < 0.0001$) with a significant region-by-tracer interaction ($P < 0.001$).

Distribution Volumes. Regional values of V_T are shown in Table 2. Using RM ANOVA, significant differences in V_T were observed between tracers ($P < 0.0001$) and between regions ($P < 0.0001$), with no tracer-by-region in-

TABLE 1
Regional Peak Uptake Times and Regional Activity Washout Rate

Region	Subregion	^{11}C-DASB			^{11}C-McN 5652		
		Peak uptake (min)	Washout* (%)	Peak specific (min)	Peak uptake (min)	Washout* (%)	Peak specific (min)
Cerebellum		29.3 ± 8.5	60.7 ± 17.0	—	41.6 ± 15.1	28.4 ± 16.0	—
Midbrain		71.3 ± 18.6	16.7 ± 15.2	70.1 ± 16.5	105.6 ± 20.7	1.8 ± 3.8	99.8 ± 21.6
Thalamus		46.3 ± 10.7	38.7 ± 19.5	48.5 ± 11.7	66.5 ± 18.2	10.9 ± 11.8	75.0 ± 28.8
Striatal region	Caudate	43.8 ± 9.8	42.0 ± 18.1	69.0 ± 17.7	67.7 ± 17.8	10.7 ± 12.3	69.0 ± 17.7
	Putamen	46.0 ± 10.7	38.9 ± 18.6	68.5 ± 17.3	69.0 ± 19.3	9.9 ± 11.0	68.5 ± 17.3
	Ventral striatum	51.7 ± 14.5	33.1 ± 19.7	51.0 ± 14.3	77.3 ± 17.1	6.1 ± 8.0	75.8 ± 13.0
Limbic region	Amygdala	59.2 ± 16.1	24.5 ± 16.3	64.6 ± 17.5	88.3 ± 22.6	3.9 ± 5.9	86.9 ± 22.2
	Entorhinal Ctx	46.0 ± 11.6	39.4 ± 19.0	45.6 ± 11.3	69.6 ± 16.9	8.7 ± 8.4	70.8 ± 18.4
	Parahippocampal gyrus	39.6 ± 8.7	47.6 ± 17.7	39.6 ± 9.0	59.6 ± 14.9	14.2 ± 11.2	62.9 ± 17.6
	Hippocampus	42.5 ± 8.8	43.8 ± 18.3	41.9 ± 9.2	63.1 ± 16.5	12.4 ± 10.7	62.7 ± 15.7
	Anterior cingulate	35.2 ± 8.6	53.3 ± 19.1	35.2 ± 8.4	51.9 ± 15.7	20.1 ± 13.5	52.7 ± 17.1
Neocortical region	DLPFC	29.4 ± 6.9	63.1 ± 16.8	25.0 ± 14.1	41.0 ± 12.3	29.2 ± 14.1	44.3 ± 17.2
	MPFC	30.2 ± 7.4	61.9 ± 17.4	30.0 ± 7.3	43.3 ± 12.2	27.1 ± 13.5	26.0 ± 22.6
	OFC	29.8 ± 9.1	62.5 ± 20.0	19.6 ± 16.8	41.0 ± 13.1	28.7 ± 13.4	17.1 ± 20.0
	Temporal Ctx	34.8 ± 8.2	53.8 ± 18.9	30.0 ± 16.6	51.3 ± 13.9	19.7 ± 12.2	31.5 ± 26.4
	Parietal Ctx	30.8 ± 6.3	61.6 ± 15.8	30.2 ± 6.3	43.1 ± 13.4	27.4 ± 14.9	30.8 ± 28.6
	Occipital Ctx	31.7 ± 7.0	58.2 ± 16.7	21.3 ± 17.8	45.0 ± 12.5	25.0 ± 12.7	27.1 ± 22.8

*Regional activity washout rate (percentage decrease from peak to last frame, 120 min).
Ctx = cortex.
Values are mean ± SD of 6 experiments per tracer.

TABLE 2
Kinetic Analysis: Rate Constants, Total Distribution Volumes, and Minimal Scanning Time

Region	Subregion	^{11}C-DASB K_1 (mL g^{-1} min^{-1})	^{11}C-DASB k_2 (min^{-1})	^{11}C-DASB V_T (mL g^{-1})	^{11}C-DASB Minimal scan time (min)	^{11}C-McN 5652 K_1 (mL g^{-1} min^{-1})	^{11}C-McN 5652 k_2 (min^{-1})	^{11}C-McN 5652 V_T (mL g^{-1})	^{11}C-McN 5652 Minimal scan time (min)
Cerebellum		0.40 ± 0.07	0.040 ± 0.010	10.1 ± 2.0	65	0.33 ± 0.03	0.016 ± 0.005	20.8 ± 3.6	35
Midbrain		0.34 ± 0.05	0.010 ± 0.002	33.2 ± 5.9	95	0.25 ± 0.01	0.005 ± 0.001	48.2 ± 9.7	95
Thalamus		0.46 ± 0.08	0.021 ± 0.005	23.0 ± 3.4	85	0.34 ± 0.02	0.010 ± 0.003	36.9 ± 7.6	55
Striatal region	Caudate	0.43 ± 0.06	0.022 ± 0.004	19.5 ± 2.6	85	0.32 ± 0.04	0.010 ± 0.003	35.5 ± 8.3	65
	Putamen	0.48 ± 0.08	0.021 ± 0.004	23.3 ± 3.8	85	0.37 ± 0.03	0.009 ± 0.002	41.3 ± 7.9	65
	Ventral striatum	0.44 ± 0.08	0.018 ± 0.004	25.7 ± 5.7	95	0.32 ± 0.02	0.008 ± 0.002	42.8 ± 8.7	75
Limbic region	Amygdala	0.30 ± 0.06	0.014 ± 0.003	22.0 ± 4.9	95	0.23 ± 0.01	0.007 ± 0.001	36.7 ± 7.2	65
	Entorhinal Ctx	0.31 ± 0.06	0.021 ± 0.005	15.0 ± 3.3	85	0.23 ± 0.02	0.009 ± 0.002	26.8 ± 4.1	85
	Parahippocampal gyrus	0.31 ± 0.05	0.026 ± 0.005	12.3 ± 1.9	85	0.25 ± 0.02	0.011 ± 0.002	23.5 ± 4.3	65
	Hippocampus	0.31 ± 0.05	0.024 ± 0.005	13.4 ± 2.0	75	0.25 ± 0.01	0.010 ± 0.002	24.9 ± 4.5	65
	Anterior cingulate	0.41 ± 0.06	0.031 ± 0.007	13.5 ± 2.2	75	0.31 ± 0.02	0.013 ± 0.003	24.5 ± 3.7	55
Neocortical region	DLPFC	0.44 ± 0.07	0.041 ± 0.009	11.0 ± 2.1	65	0.35 ± 0.03	0.017 ± 0.004	21.5 ± 3.0	45
	MPFC	0.45 ± 0.07	0.040 ± 0.009	11.5 ± 2.1	65	0.34 ± 0.03	0.016 ± 0.003	22.0 ± 2.9	55
	OFC	0.43 ± 0.08	0.043 ± 0.014	10.7 ± 2.6	75	0.33 ± 0.01	0.016 ± 0.003	20.6 ± 3.0	35
	Temporal Ctx	0.35 ± 0.06	0.032 ± 0.007	11.5 ± 2.1	75	0.28 ± 0.02	0.013 ± 0.003	22.5 ± 3.2	55
	Parietal Ctx	0.40 ± 0.06	0.039 ± 0.006	10.7 ± 1.7	65	0.33 ± 0.03	0.016 ± 0.004	21.5 ± 3.3	45
	Occipital Ctx	0.38 ± 0.07	0.036 ± 0.007	10.7 ± 1.9	75	0.32 ± 0.01	0.015 ± 0.003	21.7 ± 3.1	55

K_1 and k_2 = rate constants; V_T = total distribution volume; Ctx = cortex.
Values are mean ± SD of 6 experiments per tracer.

teraction ($P = 0.40$). ^{11}C-DASB had a lower V_T than ^{11}C-McN 5652 (16.3 mL g^{-1} compared with 28.9 mL g^{-1}, average of all regions, all subjects).

Minimal Scan Time. Table 2 lists the minimal scanning times required to reach time-independent measures of V_T for ^{11}C-DASB and ^{11}C-McN 5652 in different regions. The mean regional minimal scan time for ^{11}C-DASB (79 ± 9 min) was significantly longer than that of ^{11}C-McN 5652 (61 ± 16 min; $P < 0.001$). Figure 7 displays the biases and errors associated with shorter scan durations for each radiotracer in the region of highest SERT density (midbrain). Stable measurements of V_T in the midbrain required 95 min of data for both ^{11}C-DASB and ^{11}C-McN 5652.

Nonspecific Distribution Volumes. Values of cerebellar V_T are presented in Table 2. ^{11}C-DASB had a significantly lower cerebellar V_T than ^{11}C-McN 5652 ($P < 0.0001$). No difference was seen between subjects in the nonspecific distribution volume ($P = 0.98$). Since f_1 could not be reliably determined for ^{11}C-McN 5652, f_2 could only be determined for ^{11}C-DASB (0.92% ± 0.24%).

BP. Table 3 lists the regional values of BP for each tracer. Significant differences in BP were observed between tracers

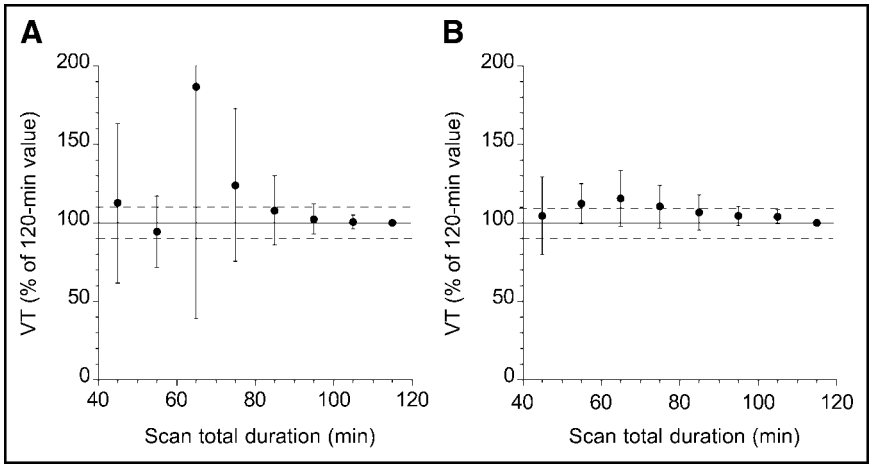

FIGURE 7. Time–stability of ^{11}C-DASB (A) and ^{11}C-McN 5652 (B) V_T in midbrain. Times refer to midtimes of each 10-min acquisition. Data of shorter duration were analyzed, and estimated midbrain V_T (mean ± SD) is expressed as percentage of value derived with complete dataset (120 min). Each point is average of 6 datasets. Deviation from 100% of mean value indicates bias associated with shorter scanning times, whereas SD indicates error associated with shorter scanning times.

TABLE 3
BP and Specific-to-Nonspecific Partition Coefficients

Region	Subregion	^{11}C-DASB BP (mL g^{-1})	^{11}C-DASB V_3''	^{11}C-DASB V_3'' normalized to midbrain (%)	^{11}C-McN 5652 BP (mL g^{-1})	^{11}C-McN 5652 V_3''	^{11}C-McN 5652 V_3'' normalized to midbrain (%)
Midbrain		19.95 ± 2.82	2.04 ± 0.44	100.0 ± 0.0	24.60 ± 7.33	1.20 ± 0.34	100.0 ± 0.0
Thalamus		12.42 ± 1.60	1.27 ± 0.29	56.2 ± 5.3	15.73 ± 4.88	0.76 ± 0.17	60.1 ± 17.2
Striatal region	Caudate	8.89 ± 0.79	0.91 ± 0.19	43.3 ± 6.3	13.66 ± 4.47	0.65 ± 0.16	53.3 ± 14.9
	Putamen	12.36 ± 1.89	1.26 ± 0.27	60.2 ± 6.8	19.13 ± 5.38	0.93 ± 0.21	76.0 ± 15.3
	Ventral striatum	14.28 ± 2.62	1.45 ± 0.31	69.1 ± 8.9	20.51 ± 5.31	1.00 ± 0.23	81.1 ± 17.7
Limbic region	Amygdala	10.76 ± 2.57	1.08 ± 0.23	50.8 ± 5.9	14.14 ± 3.23	0.69 ± 0.16	57.8 ± 7.6
	Entorhinal Ctx	4.20 ± 1.05	0.42 ± 0.10	20.6 ± 3.8	4.51 ± 2.77	0.23 ± 0.17	22.0 ± 7.3
	Parahippocampal gyrus	2.01 ± 1.06	0.22 ± 0.13	9.8 ± 4.1	2.14 ± 2.15	0.11 ± 0.11	9.2 ± 6.4
	Hippocampus	3.17 ± 0.73	0.33 ± 0.12	14.3 ± 2.9	3.66 ± 1.85	0.18 ± 0.08	14.5 ± 3.0
	Anterior cingulate	3.30 ± 1.00	0.34 ± 0.14	14.6 ± 2.9	3.59 ± 1.28	0.18 ± 0.07	13.3 ± 2.8
Neocortical region	DLPFC	1.10 ± 0.72	0.12 ± 0.09	3.9 ± 3.2	0.83 ± 1.29	0.05 ± 0.07	2.5 ± 5.3
	MPFC	1.60 ± 0.81	0.17 ± 0.11	6.1 ± 3.1	1.26 ± 1.53	0.07 ± 0.08	4.1 ± 5.8
	OFC	0.59 ± 1.04	0.06 ± 0.12	1.9 ± 5.5	−0.24 ± 2.55	0.00 ± 0.12	0.0 ± 9.6
	Temporal Ctx	1.20 ± 0.96	0.13 ± 0.12	5.8 ± 4.0	1.43 ± 2.07	0.08 ± 0.11	6.2 ± 7.1
	Parietal Ctx	0.61 ± 0.66	0.07 ± 0.08	2.6 ± 2.5	0.96 ± 1.09	0.05 ± 0.06	2.2 ± 3.3
	Occipital Ctx	0.53 ± 0.89	0.06 ± 0.10	2.8 ± 3.9	0.96 ± 1.64	0.05 ± 0.09	2.9 ± 5.1

V_3'' = specific-to-nonspecific partition coefficient; Ctx = cortex.
Values are mean ± SD of 6 experiments per tracer.

($P < 0.0001$) and between regions ($P < 0.0001$) with a significant tracer-by-region interaction ($P < 0.001$).

Specific-to-Nonspecific Partition Coefficient. Table 3 lists the regional values of V_3'' for each tracer. A significant difference was observed between tracers ($P < 0.0001$) and between regions ($P < 0.0001$) with a significant tracer-by-region interaction ($P < 0.0001$).

Regional Distribution of Binding Sites. As expected, since both radiotracers bind to the SERT, across all regions for all subjects, a significant correlation between ^{11}C-DASB V_3'' and ^{11}C-McN 5652 V_3'' was observed ($R^2 = 0.88$; $P < 0.0001$). Regional variations in V_3'' should reflect the variability in regional B_{max} since V_3'' corresponds to f_2B_{max}/K_d, and f_2 and K_d are not expected to vary between regions. As both radiotracers bind to the same population of binding sites, the relative regional distribution of V_3'' should be similar. To compare the relative V_3'' of ^{11}C-DASB with that of ^{11}C-McN 5652, regional V_3'' values were expressed as a percentage of the midbrain V_3'' (Fig. 8). A significant difference was seen in the regional percentage of midbrain V_3'' between tracers ($P < 0.0001$) and between regions ($P < 0.0001$) as well as a region-by-tracer interaction ($P < 0.0001$).

DISCUSSION

In this study, the imaging qualities of the new PET radioligand for the SERT, ^{11}C-DASB, was compared with the reference tracer, ^{11}C-McN 5652. The introduction of ^{11}C-McN 5652 as a PET radioligand suitable for use in humans (*6*) represented an important advance. Before the introduction of ^{11}C-McN 5652, only the SPECT ligand ^{123}I-2β-carbomethoxy-3β-(4-iodophenyl)tropane (^{123}I-β-CIT) was available for SERT imaging in humans. Due to its lack of selectivity, the use of ^{123}I-β-CIT for SERT measurement was restricted to the midbrain (*40*). ^{11}C-McN 5652 enabled SERT imaging not only in the midbrain but also in other regions of high SERT density, such as the

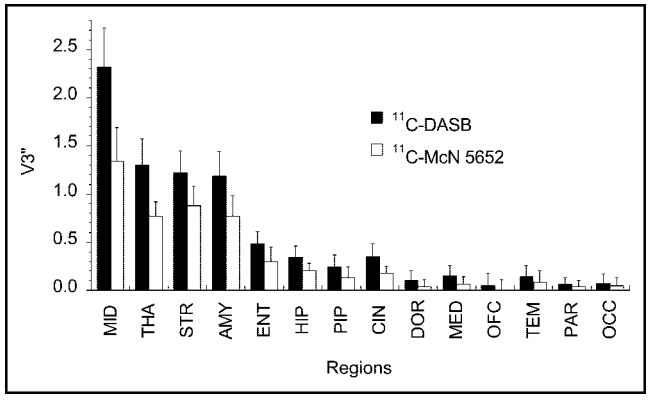

FIGURE 8. Regional V_3'' measured with ^{11}C-DASB (■) and ^{11}C-McN 5652 (□) in midbrain (MID), thalamus (THA), striatum (STR), amygdala (AMY), entorhinal cortex (ENT), hippocampus (HIP), parahippocampal gyrus (PIP), cingulate cortex (CIN), dorsolateral prefrontal cortex (DOR), medial prefrontal cortex (MED), orbitofrontal cortex (OFC), temporal cortex (TEM), parietal cortex (PAR), and occipital cortex (OCC). Values are mean ± SD ($n = 6$).

thalamus and striatum. However, the relatively low specific-to-nonspecific binding ratio of ^{11}C-McN 5652 precluded the reliable measurement of SERT in regions of moderate and low SERT density, such as the limbic and cortical regions.

Recently, Wilson et al. (*13,14*) described the synthesis and evaluation of a new class of SERT radiotracers, one of which was ^{11}C-DASB. Subsequently ^{11}C-DASB has been introduced in humans (*16,17*). Two studies compared the imaging qualities of ^{11}C-McN 5652 and ^{11}C-DASB in baboons and concluded that ^{11}C-DASB provided significant improvement over ^{11}C-McN 5652, as it provides higher specific-to-nonspecific binding ratios, higher plasma free fraction, and a faster uptake kinetics (*18,19*). The aim of this study was to determine whether the improved properties of ^{11}C-DASB observed in baboon studies were preserved in human subjects. To provide an unbiased comparison of the tracers, both tracers were studied in the same human subjects under identical experimental conditions.

Plasma Analysis

A desirable property of any brain PET radiotracer is relatively fast brain kinetics of uptake and washout, which allow for a short scanning time. This property is usually promoted by a fast peripheral metabolism and plasma clearance. The relatively slow metabolism and clearance of ^{11}C-McN 5652 contribute, among other factors, to its protracted brain uptake. Regarding metabolism rate, predictions from baboon studies were confirmed in this study. In baboons, the rate of metabolism of ^{11}C-DASB was faster than that of ^{11}C-McN 5652. For example, the parent fractions of ^{11}C-DASB and ^{11}C-McN 5652 at 30 min after injection were 20% ± 6% and 28% ± 13%, respectively. In humans, the metabolism of both tracers was slower than in baboon, but the rate of metabolism of ^{11}C-DASB remained significantly faster (32% ± 6% at 30 min) than that of ^{11}C-McN 5652 (59% ± 13% at 30 min).

In contrast, examination of the plasma clearance revealed an important difference between baboons and humans. In baboons, the clearance rate of ^{11}C-DASB (84 ± 23 L h^{-1}) was faster than that of ^{11}C-McN 5652 (58 ± 13 L h^{-1}) (n = 4 per tracer (*18*)). In humans, the clearance of ^{11}C-DASB (159 ± 34 L h^{-1}) was not significantly different from that of ^{11}C-McN 5652 (170 ± 53 L h^{-1}). After normalizing for body weight (baboon, 25 kg; human, 70 kg), the plasma clearance of ^{11}C-DASB was faster in baboons (3.36 L h^{-1} kg^{-1}) compared with that of humans (2.27 L h^{-1} kg^{-1}), whereas the clearance of ^{11}C-McN 5652 was similar in both species (baboons, 2.32 L h^{-1} kg^{-1}; humans 2.43 L h^{-1} kg^{-1}).

This species difference in plasma clearance impacted on the scanning time. In baboons, the faster plasma clearance of ^{11}C-DASB contributed to its faster brain uptake kinetics and shorter minimal scan duration. In humans, the plasma clearance of both ligands was similar, and the advantage of ^{11}C-DASB over ^{11}C-McN 5652 in terms of minimal scan duration was not observed in humans.

As previously reported, the plasma free fraction of ^{11}C-McN 5652 is not measurable with our standard technique (*7*). In contrast, the free fraction of ^{11}C-DASB was measurable, allowing for the control of this parameter in clinical studies. Without the measurement of f_1, between conditions differences in brain distribution volumes are difficult to interpret. The plasma free fraction of ^{11}C-DASB measured in this study (8.9% ± 1.6%) was similar to that reported previously in humans (11.0% ± 1.2%) (*17*) and baboons (13.5% ± 1.7%) (*18*).

Image Analysis

Inspection of the activity distribution (Fig. 4), time–activity curves (Fig. 5), and ratios to cerebellum curves (Fig. 6) reveals one of the major differences between these 2 tracers—that is, the improved signal-to-noise ratio. On the ^{11}C-DASB images, the cerebellum is darker, and the contrast between the regions rich in SERT and the cerebellum is much sharper. Examination of the midbrain on the transaxial images in Figure 4 is instructive. With tracers such as ^{123}I-β-CIT or ^{11}C-McN 5652, the midbrain appeared as a homogenous region of high binding. With ^{11}C-DASB, the higher concentration of SERT in the dorsal raphe compared with the rest of the midbrain is noticeable as high activity concentrated just above the fourth ventricule. The higher concentration of SERT in the amygdala is also visually detectable with ^{11}C-DASB but not with ^{11}C-McN 5652.

Uptake Kinetics and Scan Duration

The kinetic analysis was performed using a 1TC model for both tracers, the model of choice for both ^{11}C-McN 5652 (*5,7,8*) and ^{11}C-DASB (*17*). The value of K_1 for ^{11}C-DASB reported in this study (0.465 ± 0.08 mL g^{-1} min^{-1}) was in the same range as that reported by Ginovart et al. (*17*) in humans and about one third of that observed in baboons (*18*). The value of ^{11}C-McN 5652 K_1 in the current study (0.302 ± 0.04 mL g^{-1} min^{-1}) was in good agreement with the value reported in a previous study from our group (0.248 ± 0.37 mL g^{-1} min^{-1}) (*7*).

Compared with ^{11}C-McN 5652, ^{11}C-DASB displayed an earlier regional peak uptake and peak specific binding, and, by 90 min, more of the ^{11}C-DASB activity was cleared from the brain. Yet, the faster kinetics of ^{11}C-DASB did not translate into a shorter minimal scan duration required to derive time-independent estimates of V_T when compared with ^{11}C-McN 5652. This finding contrasts with that observed in baboons (*18*). In baboons, the regional minimal scan duration for ^{11}C-DASB was 37 ± 11 min, significantly shorter than that for ^{11}C-McN 5652 (65 ± 5 min). In humans, the regional minimal scan duration for ^{11}C-DASB was 79 ± 11 min versus 59 ± 16 min for ^{11}C-McN 5652. Thus, the regional minimal scan duration was identical in baboons and humans for ^{11}C-McN 5652, reflecting the fact that the plasma clearance of ^{11}C-McN 5652 is similar in both species. In contrast, the slower plasma clearance of ^{11}C-DASB in humans compared with baboons translated into a sizeable increase in the regional minimal scan dura-

tion. In the midbrain, the region with the highest SERT density, the time of peak specific binding was not significantly different between the 2 tracers, contributing to an identical requirement in scanning time for ^{11}C-DASB and ^{11}C-McN 5652 in this region. For both ^{11}C-DASB and ^{11}C-McN 5652, 95 min of scanning was needed to derive a time-invariant estimate of midbrain V_T.

Regarding ^{11}C-McN 5652 minimal scan duration, the findings from this study ($n = 6$) were in disagreement with the results obtained in our initial human dataset ($n = 6$), in which we observed a regional minimal scan duration of 117 ± 13 min (*7*). In the previous study, the long scan duration was due to the results from one outlier individual. Because no valid reason for removing this individual from the analysis could be identified, results were reported using the whole dataset, including the outlier. Removal of this subject would have resulted in a finding similar to that of the current study. In addition, we examined this issue in a third and larger dataset of ^{11}C-McN 5652 human scans ($n = 35$). Again, the results were identical to the present dataset. We conclude that the minimal scan duration of ^{11}C-McN 5652 was overestimated in our original study (*7*).

These considerations highlight an inherent problem when determining the minimal scanning duration based on small samples. It follows that caution must be used in the interpretation of these results for ^{11}C-DASB, which rely on data from 6 individuals. However, the results observed here for ^{11}C-DASB are relatively consistent with the time–stability results reported by Ginovart et al. ($n = 5$ (*17*)). Based on a dataset that did not include the midbrain, Ginovart et al. proposed a minimal scan duration of 80 min for ^{11}C-DASB. Based on the present dataset that includes the midbrain, we proposed a minimal scan duration of 95 min for ^{11}C-DASB.

Nonspecific Binding

The cerebellum distribution reported here for ^{11}C-McN 5652 (20.8 ± 3.6 mL g^{-1}) was similar to values reported previously by our group (17.8 ± 1.9 mL g^{-1}) (*7*). The cerebellum distribution volume of ^{11}C-DASB (10.1 ± 2.0 mL g^{-1}) was significantly lower than that of ^{11}C-McN 5652 and in good agreement with the value reported by Ginovart et al. (11.8 ± 1.5 mL g^{-1}) (*17*). The lower nonspecific distribution volume of ^{11}C-DASB compared with that of ^{11}C-McN 5652 observed here in the same human subjects confirmed a similar observation made in baboons: In that species, nonspecific distribution volumes for ^{11}C-DASB and ^{11}C-McN 5652 were 17.3 ± 0.5 mL g^{-1} and 27.7 ± 4.0 mL g^{-1}, respectively (*18*). The lower nonspecific distribution volume of ^{11}C-DASB confers on this tracer a critical advantage compared with ^{11}C-McN 5652, as the high nonspecific distribution volume of ^{11}C-McN 5652 hampers the ability to achieve high signal-to-noise ratios.

Receptor Parameters

The BP of ^{11}C-DASB was lower than that of ^{11}C-McN 5652 by 22% ± 27%. As both tracers presumably bind to the same population of sites (same B_{max}), the relative magnitude of BP will depend on the respective values of f_1 and K_d ($BP = f_1B_{max}/K_d$). In vitro, the K_d of ^{11}C-DASB is 0.87 ± 0.41 nmol/L and 1.77 ± 0.25 nmol/L at 22°C and 37°C, respectively (*18*). ^{11}C-McN 5652 K_d is 0.33 ± 0.12 and 0.26 ± 0.13 nmol/L at 22°C and 37°C, respectively (*18*). Thus, the affinity of ^{11}C-DASB for SERT is 3–7 times lower than that of ^{11}C-McN 5652. However, this large difference in K_d did not translate into a large difference in BP, because the plasma free fraction of ^{11}C-DASB is higher than that of ^{11}C-McN 5652.

The imaging qualities of a tracer are not defined by BP alone but rather by the ratio of BP to nonspecific distribution volume—that is, V_3''. For a given region, a higher value of V_3'' means an improved signal-to-noise ratio and better reliability in the measurement. The values of V_3'' for ^{11}C-McN 5652 measured in this study were in good agreement with our previously published study (*7*). However, values of ^{11}C-DASB V_3'' measured here were lower than those reported by Ginovart et al. (*17*). Note that the quantity denoted V_3'' here is denoted BP in the study of Ginovart et al. (*17*). For example, ^{11}C-DASB V_3'' in the thalamus was 1.27 ± 0.29 in this study, compared with 2.00 ± 0.34 in the Ginovart study (*17*). ^{11}C-DASB V_3'' in the occipital cortex was 0.06 ± 0.10 in this study, compared with 0.51 ± 0.09 in the Ginovart study (*17*). The reasons for these differences are not obvious, as the same analytic method was used to derive V_T and V_3'' (1TC model). This difference is presumably due to the method used to define ROIs and cerebellum boundaries and highlights the difficulties in comparing V_3'' data across groups.

^{11}C-DASB V_3'' values, though lower than previously reported in Ginovart et al. (*17*), were significantly higher than V_3'' values of ^{11}C-McN 5652. Combining all regions, the V_3'' values for ^{11}C-DASB was increased by 74% ± 33% compared with those for ^{11}C-McN 5652. This result is similar to that observed in baboon. In that species, ^{11}C-DASB V_3'' values were found to be 42% ± 29% higher than that of ^{11}C-McN 5652 (*18*). This higher signal-to-noise ratio of ^{11}C-DASB compared with that of ^{11}C-McN 5652 is due to lower nonspecific binding rather than higher BP and is the most clinically significant difference between the tracers. Due to this enhanced signal-to-noise ratio, ^{11}C-DASB should allow for a more reliable quantification of SERT parameters in regions of moderate SERT densities, such as the limbic regions. However, in our hands, values of V_3'' with ^{11}C-DASB are still very low in neocortical regions ($V_3'' < 0.2$), and it is unlikely that ^{11}C-DASB would be able to provide a reliable measurement of SERT in these brain areas.

When comparing the V_3'' values for each tracer across regions, a significant tracer-by-region interaction was observed. This interaction was unexpected and reminiscent of a similar finding in baboons (*18*). To explore this issue further, regional V_3'' values were normalized for each tracer to the midbrain V_3'' value. Assuming that both tracers bind to the same population of receptors, and that, for each tracer, K_d and nonspecific distribution volumes are constant across

regions, the normalized V_3'' values should be identical for both tracers. In general, this prediction was confirmed (Table 3). However, as seen in baboons, the normalized V_3'' value for ^{11}C-McN 5652 was greater in the striatal regions than that of ^{11}C-DASB. The reason for this discrepancy was not clear and might be due to regional differences in nonspecific binding. Another possibility would be that, in the striatum, ^{11}C-McN 5652 exhibits significant binding to an as yet unidentified receptor.

CONCLUSION

The newly developed SERT radiotracer ^{11}C-DASB was compared with the reference tracer ^{11}C-McN 5652 in the same human subjects, under identical experimental conditions. In baboons, 3 critical advantages of ^{11}C-DASB were observed: (a) higher specific-to-nonspecific equilibrium activity ratios—that is, higher V_3''; (b) measurable plasma free fraction; and (c) faster brain uptake kinetics and shorter minimal scan duration. Two of 3 of these improvements were confirmed in humans: (a) regional ^{11}C-DASB V_3'' values were significantly higher; and (b) ^{11}C-DASB plasma free fraction was measurable with the conventional ultracentrifugation method. However, the plasma clearance of ^{11}C-DASB was significantly slower in humans than in baboons, and, in humans, the minimal scan duration of ^{11}C-DASB was not shorter than that of ^{11}C-McN 5652. From this comparative evaluation, ^{11}C-DASB emerged as the tracer of choice for the quantification of SERT, an advantage that should be mostly relevant to the study of SERT in the limbic regions. Additional research is needed to develop a radioligand that will enable the examination of SERT in neocortical regions.

ACKNOWLEDGMENTS

This work was supported in part by grants from the National Alliance for Research on Schizophrenia and Depression, the National Institute of Mental Health (1 R21 MH66624-01, 1-K02-MH01603-01), and the Lieber Center for Schizophrenia Research at Columbia University. The authors thank Alan Wilson for providing the precursor for ^{11}C-DASB and acknowledge the technical assistance of Julie Arcement, Jennifer Bae, Susan Curry, Ashlie Darr, Ingrid Gelbard-Strokes, Charisse Green, Elizabeth Hackett, Kimchung Ngo, Chaka Peters, Ben Poletta, Nurat Quadri, Norman Simpson, Lyudmila Savenkova, Kris Wolff, and Zohar Zephrani.

REFERENCES

1. Laruelle M, Vanisberg M, Maloteaux J. Regional and subcellular localization in human brain of [^{3}H]paroxetine binding, a marker of serotonin uptake sites. *Biol Psychiatry.* 1988;24:299–309.
2. Backstrom I, Bergstrom M, Marcusson J. High affinity [^{3}H]paroxetine binding to serotonin uptake sites in human brain tissue. *Brain Res.* 1989;486:261–268.
3. Plenge P, Mellerup ET, Laursen H. Regional distribution of the serotonin transport complex in human brain, identified with ^{3}H-paroxetine, ^{3}H-citalopram and ^{3}H-imipramine. *Prog Neuropsychopharmacol Biol Psychiatry.* 1990;14:61–72.
4. Suehiro M, Scheffel U, Ravert HT, Dannals RF, Wagner H Jr. [^{11}C](+)McN5652 as a radiotracer for imaging serotonin uptake sites with PET. *Life Sci.* 1993;53:883–892.
5. Szabo Z, Scheffel U, Mathews WB, et al. Kinetic analysis of [^{11}C]McN5652: a serotonin transporter radioligand. *J Cereb Blood Flow Metab.* 1999;19:967–981.
6. Szabo Z, Kao PF, Scheffel U, et al. Positron emission tomography imaging of serotonin transporters in the human brain using [^{11}C](+)McN5652. *Synapse.* 1995;20:37–43.
7. Parsey RV, Kegeles LS, Hwang DR, et al. In vivo quantification of brain serotonin transporters in humans using [^{11}C]McN 5652. *J Nucl Med.* 2000;41:1465–1477.
8. Buck A, Gucker PM, Schonbachler RD, et al. Evaluation of serotonergic transporters using PET and [^{11}C](+)McN-5652: assessment of methods. *J Cereb Blood Flow Metab.* 2000;20:253–262.
9. Ichimiya T, Suhara T, Sudo Y, et al. Serotonin transporter binding in patients with mood disorders: a PET study with [^{11}C](+)McN5652. *Biol Psychiatry.* 2002;51:715–722.
10. Simpson HB, Lombardo I, Slifstein M, et al. Serotonin transporters in obsessive compulsive disorder: a positron emission tomography study with [^{11}C]McN 5652. *Biol Psychiatry.* 2003;54:1414–1421.
11. McCann UD, Szabo Z, Scheffel U, Dannals RF, Ricaurte GA. Positron emission tomographic evidence of toxic effect of MDMA ("ecstasy") on brain serotonin neurons in human beings. *Lancet.* 1998;352:1433–1437.
12. Buchert R, Thomasius R, Nebeling B, et al. Long-term effects of "ecstasy" use on serotonin transporters of the brain investigated by PET. *J Nucl Med.* 2003;44:375–384.
13. Wilson AA, Ginovart N, Schmidt M, Meyer JH, Threlkeld PG, Houle S. Novel radiotracers for imaging the serotonin transporter by positron emission tomography: synthesis, radiosynthesis, and in vitro and ex vivo evaluation of ^{11}C-labeled 2-(phenylthio)araalkylamines. *J Med Chem.* 2000;43:3103–3110.
14. Wilson AA, Houle S. Radiosynthesis of carbon-11 labelled N-methyl-2(arylthio) benzylamines: potential radiotracers for the serotonin reuptake receptor. *J Labelled Compds Radiopharm.* 1999;42:1277–1288.
15. Wilson AA, Ginovart N, Hussey D, Meyer J, Houle S. In vitro and in vivo characterisation of [^{11}C]-DASB: a probe for in vivo measurements of the serotonin transporter by positron emission tomography. *Nucl Med Biol.* 2002;29:509–515.
16. Houle S, Ginovart N, Hussey D, Meyer J, Wilson A. Imaging the serotonin transporter with positron emission tomography: initial human studies with [^{11}C]DAPP and [^{11}C]DASB. *Eur J Nucl Med.* 2000;27:1719–1722.
17. Ginovart N, Wilson AA, Meyer JH, Hussey D, Houle S. Positron emission tomography quantification of [^{11}C]-DASB binding to the human serotonin transporter: modeling strategies. *J Cereb Blood Flow Metab.* 2001;21:1342–1353.
18. Huang Y, Hwang DR, Narendran R, et al. Comparative evaluation in nonhuman primates of five PET radiotracers for imaging the serotonin transporters: [^{11}C]McN 5652, [^{11}C]ADAM, [^{11}C]DASB, [^{11}C]DAPA, and [^{11}C]AFM. *J Cereb Blood Flow Metab.* 2002;22:1377–1398.
19. Szabo Z, McCann UD, Wilson AA, et al. Comparison of (+)-^{11}C-McN5652 and ^{11}C-DASB as serotonin transporter radioligands under various experimental conditions. *J Nucl Med.* 2002;43:678–692.
20. Langstrom B, Antoni G, Gullberg P, et al. Synthesis of L- and D-[methyl-^{11}C]methionine. *J Nucl Med.* 1987;28:1037–1040.
21. Zessin J, Gucker P, Ametamey S, et al. Efficient synthesis of the enantiomerically pure thioester precursors of [^{11}C]McN-5652 from racemic McN-5652. *J Labelled Compds Radiopharm.* 1999;42:1301–1312.
22. Huang YY, Mahmood K, Simpson NR, Mason NS, Mathis CA. Stereoconservative synthesis of the enantiomerically pure precursors of [C-11](+)-McN 5652 and [C-11](-)-McN 5652. *J Labelled Compds Radiopharm.* 1998;41:9–17.
23. Mawlawi OM, Weiss R, Shinn A, Pidcock J, Slifstien M, Laruelle M. Performance characteristics of a head immobilization device for PET imaging [abstract]. *J Nucl Med.* 1999;40(suppl):281P.
24. Abi-Dargham A, Simpson N, Kegeles L, et al. PET studies of binding competition between endogenous dopamine and the D1 radiotracer [^{11}C]NNC 756. *Synapse.* 1999;32:93–109.
25. Abi-Dargham A, Laruelle M, Seibyl J, et al. SPECT measurement of benzodiazepine receptors in human brain with [123-I]iomazenil: kinetic and equilibrium paradigms. *J Nucl Med.* 1994;35:228–238.
26. Gandelman MS, Baldwin RM, Zoghbi SS, Zea-Ponce Y, Innis RB. Evaluation of ultrafiltration for the free fraction determination of single photon emission computerized tomography (SPECT) radiotracers: β-CIT, IBF and iomazenil. *J Pharm Sci.* 1994;83:1014–1019.
27. Abi-Dargham A, Martinez D, Mawlawi O, et al. Measurement of striatal and extrastriatal dopamine D1 receptor binding potential with [^{11}C]NNC 112 in humans: validation and reproducibility. *J Cereb Blood Flow Metab.* 2000;20:225–243.

28. Woods RP, Cherry SR, Mazziotta JC. Rapid automated algorithm for aligning and reslicing PET images. *J Comput Assist Tomogr.* 1992;16:620–633.
29. Duvernoy H. *The Human Brain: Surface, Three-Dimensional Sectional Anatomy and MRI*. New York, NY: Sringer-Verlag; 1991.
30. Talairach J, Tournoux P. *Co-Planar Stereotactic Atlas of the Human Brain: Three-Dimensional Proportional System—An Approach of Cerebral Imaging*. New York, NY: Theime Medical; 1988.
31. Killiany RJ, Moss MB, Nicholson T, Jolez F, Sandor T. An interactive procedure for extracting features of the brain from magnetic resonance images: the lobes. *Human Brain Mapping.* 1997;5:355–363.
32. Kates WR, Abrams MT, Kaufmann WE, Breiter SN, Reiss AL. Reliability and validity of MRI measurement of the amygdala and hippocampus in children with fragile X syndrome. *Psychiat Res Neuroimag.* 1997;75:31–48.
33. Pani L, Gessa GL, Carboni S, Portas CM, Rossetti ZL. Brain dialysis and dopamine: does the extracellular concentration of dopamine reflect synaptic release? *Eur J Pharmacol.* 1990;180:85–90.
34. Mawlawi O, Martinez D, Slifstein M, et al. Imaging human mesolimbic dopamine transmission with positron emission tomography. I. Accuracy and precision of D2 receptor parameter measurements in ventral striatum. *J Cereb Blood Flow Metab.* 2001;21:1034–1057.
35. Mintun MA, Raichle ME, Kilbourn MR, Wooten GF, Welch MJ. A quantitative model for the in vivo assessment of drug binding sites with positron emission tomography. *Ann Neurol.* 1984;15:217–227.
36. Laruelle M, Baldwin RM, Rattner Z, et al. SPECT quantification of [^{123}I]iomazenil binding to benzodiazepine receptors in nonhuman primates. I. Kinetic modeling of single bolus experiments. *J Cereb Blood Flow Metab.* 1994;14:439–452.
37. Koeppe RA, Holthoff VA, Frey KA, Kilbourn MR, Kuhl DE. Compartmental analysis of [^{11}C]flumazenil kinetics for the estimation of ligand transport rate and receptor distribution using positron emission tomography. *J Cereb Blood Flow Metab.* 1991;11:735–744.
38. Levenberg K. A method for the solution of certain problems in least squares. *Q Appl Math.* 1944;2:164–168.
39. Laruelle M, van Dyck C, Abi-Dargham A, et al. Compartmental modeling of iodine-123-iodobenzofuran binding to dopamine D_2 receptors in healthy subjects. *J Nucl Med.* 1994;35:743–754.
40. Laruelle M, Baldwin RM, Malison RT, et al. SPECT imaging of dopamine and serotonin transporters with [^{123}I]b-CIT: pharmacological characterization of brain uptake in nonhuman primates. *Synapse.* 1993;13:295–309.

JNM The Journal of NUCLEAR MEDICINE

Comparative Evaluation of Serotonin Transporter Radioligands ^{11}C-DASB and ^{11}C-McN 5652 in Healthy Humans

W. Gordon Frankle, Yiyun Huang, Dah-Ren Hwang, Peter S. Talbot, Mark Slifstein, Ronald Van Heertum, Anissa Abi-Dargham and Marc Laruelle

J Nucl Med. 2004;45:682-694.

The Journal of Nuclear Medicine is published monthly.
SNMMI | Society of Nuclear Medicine and Molecular Imaging
1850 Samuel Morse Drive, Reston, VA 20190.
(Print ISSN: 0161-5505, Online ISSN: 2159-662X)

SNMMI SOCIETY OF NUCLEAR MEDICINE AND MOLECULAR IMAGING